Substituting soybean oil-based polyol into polyurethane flexible foams

Ling Zhang [a], Hyun K. Jeon [a,1], Jeff Malsam [b], Ron Herrington [c], Christopher W. Macosko [a,*]

[a] *Department of Chemical Engineering and Material Science, University of Minnesota, Minneapolis, MN 55455, United States*
[b] *Process Solutions Technology Development Center, Cargill Inc., Wayzata, MN 55391, United States*
[c] *Ron Herrington Consultancy, 2919 County Road 510, Brazoria, TX 77422, United States*

Abstract

Polyurethane (PU) flexible foams were synthesized by substituting a portion of base polyether polyol with soybean oil-derived polyol (SBOP) as well as well-known substituent: crosslinker polyol and styrene acrylonitrile (SAN) copolymer-filled polyol. Increases in compression modulus were observed in all substituted foams and the most substantial increase was found in the 30% SBOP-substituted sample. Scanning electron microscopy (SEM) was used to examine cellular structure, in particular cell size. Polymer phase morphology, i.e., interdomain spacing and microphase separation, was studied using small-angle X-ray scattering (SAXS) and atomic force microscopy (AFM). Hydrogen bonding was investigated via Fourier transform infrared (FTIR) spectroscopy. Thermal and mechanical behaviors of foams were examined using dynamic mechanical analysis (DMA) and differential scanning calorimetry (DSC). Compression properties were tested and compared via a 65% indentation force deflection (IFD) test. It was found that substituting SAN-filled polyol slightly reduced foam cell size and had no effect on polymer phase morphology. Crosslinker and SBOP polyols, on the other hand, had appreciable influence on polymer phase morphology. Crosslinker polyol disrupted hydrogen bonding between hard segments and was mixed with hard domains. SBOP polyol reduced hard domain size and soft domain fraction, and showed a broad distribution of interdomain spacings. Compression modulus increases in foams correlated well with shear modulus by DMA and could be associated with the polymer phase morphology changes.
© 2007 Elsevier Ltd. All rights reserved.

Keywords: Polyurethane foam; Morphology; Soybean oil polyol

1. Introduction

Polyurethane (PU) is one of the most versatile polymeric materials with regard to both processing methods and mechanical properties. By proper selection of reactants, the resulting PU can be, for example, a rigid crystalline plastic, flexible elastomer, or viscoelastic gel. This wide range of achievable properties makes PU an indispensable component in building construction, consumer products, transportation and medical devices [1,2]. Similar to nearly all polymeric materials, PU relies on petroleum oil as the feedstock for its major components: hydroxyl-containing polyols and isocyanates. Over the past decade, as the price of petroleum oil escalated, the stability and the sustainability of the petroleum market have become growing concerns. Costs of polymeric raw materials have since risen steadily as a result of rising feedstock price [3]. In contrast to the less predictable petroleum market, agricultural products, such as vegetable oils, have not only maintained steady prices, but also experienced surpluses. In US from 1985 to 2007 the price of soybean oil has risen 50% from 19 ¢ to 28 ¢/lb whereas the price of crude oil has soared from 7 ¢ to 18 ¢/lb, a more than 150% increase [4].

Developing bio-renewable feedstocks for PU manufacturing and for the polymer industry as a whole becomes highly desirable for both economic and environmental reasons [5]. In PU manufacturing, vegetable oils can be potential replacements for polyols. However, to form PU, hydroxyl groups are required to react with isocyanate. With the exception of castor and lesquerella oils, vegetable oils do not bear hydroxyls

---

naturally. Several methods are currently known to add hydroxyls at the unsaturated sites: hydroformylation followed by hydrogenation [6], epoxidation followed by oxirane opening [7], ozonolysis followed by hydrogenation [8], and microbial conversion [9]. All these methods produce polyols but with structural differences. For illustration purposes, Fig. 1 shows schematically the polyols that can be derived from a single vegetable oil triglyceride using aforementioned processes assuming no coupling or side reactions.

Researchers have successfully synthesized PU elastomers using vegetable oil-derived polyols and observed improvements in both thermal stability and oxidation resistance [10–12]. The success in incorporating vegetable oil-based polyols in PU elastomer synthesis has generated interest in using the same polyols in PU foams. Foams constitute more than 60% of all PU products, while elastomers make up 16% [13]. The

use of vegetable oil-derived polyols in foam synthesis is not only desirable but also critical in reducing petroleum components in PU.

Thus far, processed vegetable oils, such as palm, rapeseed, and soybean oil, have been used to synthesize *rigid* foams. The resulting products not only exhibit improved thermal stability but also share comparable mechanical properties with their petroleum-based analogues [14–16]. Nevertheless, the same studies also expressed concerns over low reactivity of oil-derived polyols and difficulty in foam density control.

The largest PU production goes into *flexible* foam, thus use of bio-renewable polyols for *flexible* foams is much more desirable. A direct approach is to use the natural polyol — castor oil. Foams made solely from this natural polyol are low in resiliency and have a temperature dependent modulus [17]. The narrow range of achievable foam properties and the relatively high cost of castor oil have turned researchers to processed oils for polyols. John and co-workers synthesized flexible foam using entirely soybean oil-derived polyol (SBOP) and the data indicated that improvements in both surfactant efficiency and SBOP reactivity were needed [18]. Partial incorporation of vegetable oil-derived polyols has been much more successful [19–21]. Not only have good quality foams been made, but also higher resiliency has been achieved with these foams. Among all partially substituted foams, higher hardness/compressive modulus has been consistently observed. In the study done by Herrington and Malsam, they replaced up to 30% of the total polyol with SBOP and did *not* encounter common issues associated with similar oil-derived polyols, such as odor, density control and SBOP reactivity. More remarkably, a significant load bearing increase measured by indentation force deflection test (IFD) was reported [19].

In this work, we examined foam morphology to elucidate the source of increased compressive modulus reported by Herrington and Malsam. A series of flexible foams were prepared by replacing up to 30% of petroleum-derived polyether polyol with three substituent polyols: styrene acrylonitrile (SAN) copolymer-filled, crosslinker, and SBOP polyols. Several experimental techniques were applied to characterize the samples including scanning electron microscopy (SEM), small-angle X-ray scattering (SAXS), atomic force microscopy (AFM), dynamic mechanical analysis (DMA), differential scanning calorimetry (DSC), and Fourier transform infrared (FTIR) spectroscopy. The effects of substituent polyols on both cellular structure and polymer phase morphology were examined and compared. The two substituent polyols: SAN copolymer-filled and crosslinker polyols were included in this work because use of either polyol is known to increase compressive modulus of flexible foam [2].
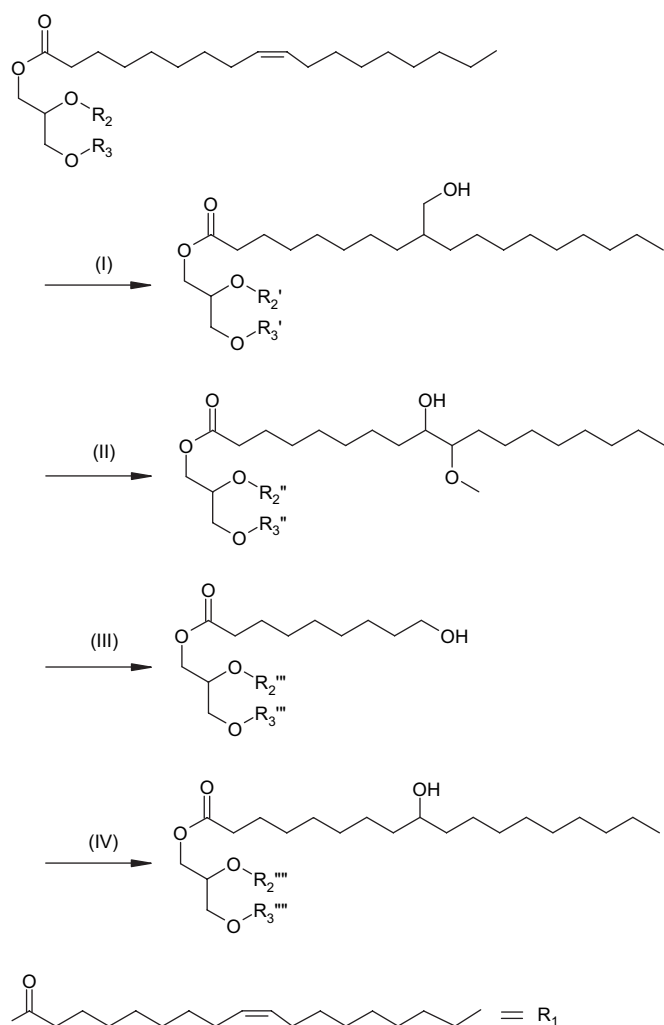

Fig. 1. A simplified schematic representation of the multistep reactions used to derive polyols from vegetable oil: (I) hydroformylation followed by hydrogenation [6]; (II) epoxidation followed by oxirane ring-opening (methanol, as an example) [7]; (III) ozonolysis followed by hydrogenation [8]; (IV) microbial conversion [9]. Vegetable oils, such as soybean oil, contain a mixture of fatty acids. In the figure, R_1 is oleic acid residue, R_2 and R_3 can be oleic, linoleic, linolenic, palmic and other related acid residues. R_2 and R_3 with superscripts represent modified fatty acid residues.

2. Experimental

2.1. Materials

Three commercially available petroleum-derived polyols, Hyperlite® E-848 (Bayer Corporation), Hyperlite® E-849 (Bayer Corporation), and Voranol® 446 (Dow Chemical
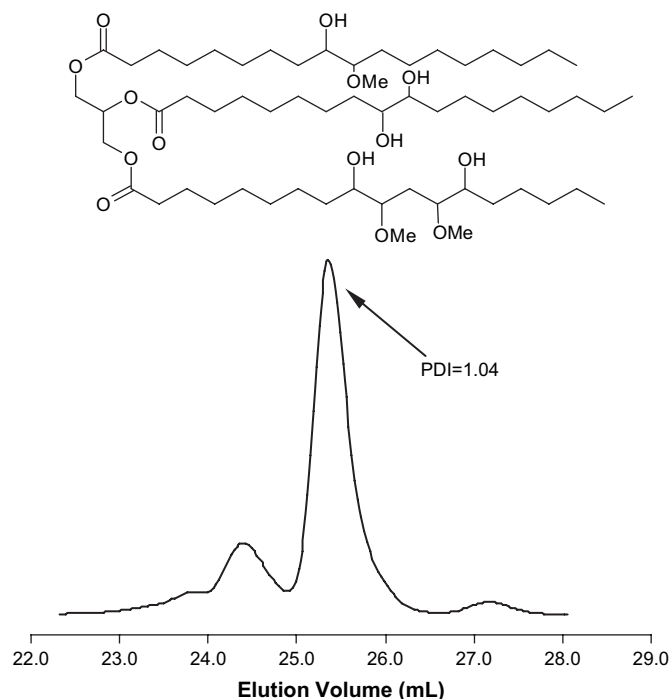
Fig. 2. Idealized structure of SBOP (top) and GPC trace of SBOP used in study (bottom).

Company), were selected. These are typical molded flexible foam polyols. Hyperlite® E-848 is a propylene oxide-based, ethylene oxide capped polyol with a number average molecular weight (M_n) of 6700 g/mol and a functionality (f_n) of 3.8 [22]. Approximately 85% of the hydroxyls in Hyperlite® E-848 are primary. Hyperlite® E-849 is a copolymer-filled polyol, based upon Hyperlite® E-848. It contains an estimated 43 wt% of stabilized styrene acrylonitrile (SAN) particles that are approximately 0.5 µm in size. Voranol® 446, referred to as a crosslinker polyol, is a low molecular weight ($M_n = 570$ g/mol) propylene oxide-based polyol with an f_n of 4.5 [23].

SBOP used in this study was synthesized by epoxidizing soybean oil followed by an oxirane ring-opening reaction using a mixture of water and methanol. Detailed synthesis procedures are described in Ref. [7]. An *idealized* structure of SBOP shown in Fig. 2 has an $M_n = 1058$ g/mol and $f_n = 5$. The actual molecular weight of SBOP used in this study was measured by gel permeation chromatography (GPC) at room temperature using known molecular weight polyether polyols as standards. Fig. 2 shows the GPC trace of SBOP. The calculated M_n of SBOP used in this study is 1060 g/mol, polydispersity index (PDI) = 1.04 for the large peak in figure and $f_n = 3.8$. The lower f_n in the actual SBOP is due to both variations in fatty acid

substituent and oligomerization of a small fraction of SBOP during modification evidenced by a second broad peak in GPC.

Toluene diisocyanate (TDI) used is an 80:20 mixture of 2,4 and 2,6 isomers (Grade A Mondur® T-80, Bayer). Isocyanate in excess of that needed to react with the OH groups on the polyols reacts with distilled water to form CO_2, which acts as the only foam blowing agent. Gelling and blowing catalysts, Dabco® 33-LV and Dabco® BL-11, were obtained from Air Products and used as-received. Dabco® 33-LV, which accelerates the reaction of NCO with OH, is a solution of 33 wt% triethylene diamine in dipropylene glycol. Dabco® BL-11, which accelerates the reaction of NCO with water, is a solution of 70 wt% bis(2-dimethylaminoethyl)ether in dipropylene glycol. Diethanolamine (DEOA, Huntsman) was used in small quantities as a foam stabilizing cross-linking agent.

Three surfactants were employed in this study: Niax® Y-10184, Dabco® DC-5169, and Tegostab® B-4690. Niax® Y-10184 (Momentive Performance Materials, formerly GE Silicones) is a silicon-based, molded foam surfactant which is used in the foam formulations not containing SBOP. Dabco® DC-5169 (Air Products) and Tegostab® B-4690 (Degussa AG) were used together in SBOP foams at a weight ratio of 1:3.

2.2. Foam synthesis

Table 1 gives the formulations used to prepare the foam samples. The amount of each component was based on 100 parts by weight of total polyol and a total mixture weight of 500 g. The amounts of TDI stoichiometrically balance NCO and reactive hydrogen species, i.e., isocyanate index = 100.

All ingredients, except TDI, were weighed into a 33-ounce paper cup (Model DMC-33, International Paper Company) and mixed using a 10-inch shop drill (Delta ShopMaster, Model DP-200) equipped with a 3-inch diameter mixing blade (ConnBlade Brand, Model ITC) for 24 s at 1100 rpm. At the end of the mixing period, pre-measured isocyanate was added to the cup and the mixing continued for additional 6 s. The contents were then quickly transferred to a pre-heated aluminum mold (38.1 × 38.1 × 11.4 cm) controlled at 66 ± 1 °C. The foam was allowed to rise and cure for 6 min, after which the foam was removed from the mold and hand crushed to open the cell windows and prevent shrinkage of the foam. Further tests were done after the foam had aged at 25 °C in 50% relative humidity for a minimum of 7 days.

The differences in polyol functionality and molecular weight lead to variations in hard-segment (HS) and soft-segment (SS) contents and will be discussed further in later sections. The HS and SS contents were calculated using Eqs. (1) and (2):

$$\%HS = \frac{EM_{H_2O}\left(EW_{H_2O} + EW_{TDI} - \frac{1}{2}W_{CO_2}\right) + EM_{DEOA}(EW_{TDI} + EW_{DEOA}) + EM_{OH}(EW_{TDI})}{W_{Tot} - EM_{H_2O}\left(\frac{1}{2}W_{CO_2}\right)} \tag{1}$$

Table 1
Foam formulation in parts by weight[a] and resultant properties

Component	Control	30% SAN[b]	10% Crosslinker	10% SBOP	30% SBOP
Hyperlite® E-848	100	70	90	90	70
Hyperlite® E-849	−	30	−	−	−
Voranol® 446	−	−	10	−	−
SBOP	−	−	−	10	30
TDI weight (g, index = 100)	156.9	155.5	170.4	161.5	172.4
HS (%)	30.0	29.7	33.0	31.1	33.4
HS-to-SS ratio	0.44	0.49	0.50	0.46	0.52
Sol fraction (%)	1.31 ± 0.20	4.75 ± 0.37	1.52 ± 0.17	1.31 ± 0.27	1.38 ± 0.18
Airflow (scfm)	2.5	3.1	2.4	4.3	3.1
Δc_p (J/g/°C)	0.33	0.25	0.23	0.16	0.14
G' at 25 °C (10^{-3} Pa)	10.5	17.7	23.2	23.5	51.8
65% IFD (kPa)	8.0	11.1	10.6	10.3	18.6

Density of all foams: 32 kg/m³.

[a] All formulations contain distilled water (4.2 pph), DEOA (1.2 pph), Dabco® 33-LV (0.35 pph), Dabco® BL-11 (0.08 pph) and surfactant (1.0 pph). Surfactant used in SBOP-containing foams is a mixture of Dabco® DC-5169 and Tegstab® B-4690 at 1:3 by weight; all other foams used Niax® Y-10184.

[b] SAN particles (8.5 wt%) in foam.

$$\%SS = \frac{EM_{OH}(EW_{OH})}{W_{Tot} - EM_{H_2O}(\frac{1}{2}W_{CO_2})} \qquad (2)$$

where EM is moles of functional group, EW is equivalent molecular weight, W is molecular weight, and subscripts H_2O, TDI, CO_2, DEOA, OH and Tot refer to water, toluene diisocyanate, carbon dioxide, diethanolamine, polyol and total, respectively. It is assumed that HS is formed via the reaction of TDI with water, DEOA, and OH on polyol, and corrected for carbon dioxide loss. SS comprises polyols. Both HS concentrations and HS-to-SS ratios are tabulated in Table 1. Note that for the 30% SAN sample the weight of the SAN particles, 8.5%, is considered neither as HS nor as SS.

2.3. Characterization

2.3.1. Solvent extraction

Small cubic samples were cut from the center of foam buns, dried at 60 °C for 24 h and weighed (0.1−0.2 g). The dried samples were then immersed in 20 ml dimethyl formamide (DMF) for 7 days at room temperature followed by drying in a vacuum oven at 60 °C for 10 days. The weight loss after solvent extraction is reported based upon an average of six samples per foam.

2.3.2. Scanning electron microscope (SEM)

Foam was frozen in liquid nitrogen and cut with a razor blade into rectangular slices: $7 \times 10 \times 2$ mm. The top surface of each slice was sputter coated with 50 Å grain-sized platinum. Cellular structure images were obtained using a scanning electron microscope (JSM-6500, JEOL) operated at 5 kV. An average of 6−8 images were collected on each foam. The perimeters of cells were manually traced from the SEM micrographs using UTHSCSA ImageTool software (Microsoft Corporation). Individual cell size was then calculated by approximating the cells as circular shapes [24,25]. Average cell diameter and cell size standard deviation were calculated from a survey of over 40 cells.

2.3.3. Dynamic mechanical analysis (DMA)

Foam disks (25 (D) × 10 mm) were tested in sinusoidal oscillation mode between two 25-mm diameter serrated parallel plates (ARES II, TA Instruments). Contact was maintained by applying a constant normal force of 50 g throughout the experiment. Storage modulus (G') was recorded at a frequency of 1 Hz over the temperature range from −100 to 200 °C. The temperature ramp rate was controlled at 3 °C/min and strain applied was 0.2% for temperature above 25 °C and 0.1% for temperature below 25 °C. Both strains are within the linear viscoelastic region of the foam in the corresponding temperature ranges.

2.3.4. Differential scanning calorimetry (DSC)

Soft-segment (SS) glass transition temperatures were determined using a DSC (Q1000, TA Instruments). Approximately 6−10 mg of foam was loaded into an aluminum pan and sealed hermetically. The sample was first heated at 10 °C/min to 110 °C and equilibrated for 2 min, followed by cooling to −120 °C and holding for 10 min before heating up to 300 °C at 10 °C/min. Glass transition temperatures and heat capacity changes were determined on the second heating cycles.

2.3.5. Small-angle X-ray scattering (SAXS)

About 10 mg of the foam sample was compressed in a copper sample holder to a thickness of 2 mm and placed in a SAXS apparatus. The setup comprises a Rigaku rotating anode, Cu source and a Siemens Hi-Star multi-wire area detector. The X-ray generator was operated at 12 kW and 40 mA. The attainable scattering angle ($\theta/2$) ranges from 0.18° to 38°. The foam was exposed to X-rays for 5 min. The raw data were normalized for sample thickness variation.

2.3.6. Atomic force microscopy (AFM)

A two-platen hydraulic press (Carver, Auto Series, Model 3895) capable of a maximum pressure of 60 MPa was used to compress $10 \times 10 \times 5$ mm foam samples into solid elastomeric sheets that are ∼200 μm thick. The foam samples were

placed between two $30 \times 30 \times 0.2$ cm highly polished (grain size < 1 μm) stainless steel plates (type 304), then held under 1.2 MPa plate-pressure at 110 ± 1 °C for 3 h [26]. The resulting elastomer sheets are semi-transparent.

Tapping mode images were obtained using an AFM (Nanoscope III Multimode, Digital Instrument) equipped with an optical microscope (Nikon) and a charge-coupled device camera. The cantilever is a standard Si cantilever with a tip radius of about 100 Å and resonance oscillating frequency of ∼275 kHz. All AFM images were acquired at ambient conditions. Cantilever was operated within the repulsive regime and images were collected at a resolution of 512×512 pixels.

2.3.7. Fourier transform infrared spectroscopy with attenuated total reflectance (FTIR-ATR)

An FTIR (Nicolet Series II Magna-750, Nicolet/Thermoelectron) equipped with a single bounce ATR attachment (Profilir™, SpectraTech) and a mercury–cadmium–telluride detector was used to collect spectra at foam surfaces. Two sets of samples, $5 \times 5 \times 1$ cm, were cut from the center of foam buns and each set comprises five different foam samples. The first set was dried under vacuum at 60 °C for 48 h prior to measurements while the second set was measured as is. Sample drying was to ensure no water adsorbed on the foam surface after curing in 50% humidity conditions. The sample was pressed against the zinc–selenium (ZnSe) ATR crystal to ensure complete contact. A total of 512 scans were taken on each sample over the wavelength range from 4000 to 400 cm^{-1} at a resolution of 4 cm^{-1}. For each foam, three ATR-IR spectra were collected at different locations of the sample to verify sample uniformity. All spectra were normalized with respect to the absorbance of the aromatic C=C stretching at 1600 cm^{-1}. Comparison between the FTIR results of two sets of foams, pre-dried and not dried, showed no difference. Deconvolution of spectrum was performed in the carbonyl region (1550–1800 cm^{-1}) using Thermo-Galactic's GRAM32 software. Each peak was fit to a Gaussian curve at a series of fixed wavelengths given in Table 2.

2.3.8. Indentation force deflection (IFD) test

One of the crucial properties of PU flexible foam is its ability to provide support under compression, commonly known as load bearing capability. This load bearing capability is measured using an indentation force deflection (IFD) test. Foam samples of $38.1 \times 38.1 \times 11.4$ cm were tested in accordance with standard procedures described in ASTM D-3574 test

B1. The sample was compressed at 5 cm/min until it reached 65% deflection. While holding the deflection constant, the foam was allowed to equilibrate for 60 s before the force was recorded. IFD test results are shown in Table 1.

3. Results and discussion

3.1. Solvent extraction

The solvent extraction was conducted to determine polymer network connectivity in foams. The measured sol fractions of the foams are tabulated in Table 1. All of the foams, with the exception of 30% SAN, have less than 2% extractables. The low extractable content is remarkable in both SBOP foams. Since SBOP contains a small amount of saturated fatty acid that cannot be functionalized, one would expect an increasing sol fraction with an increasing concentration of SBOP [27]. Furthermore, SBOP is a less reactive polyol due to its secondary hydroxyl groups. However, a low sol fraction was observed consistently in both SBOP-containing foams. It appears that the concentration of non-functional polyol in SBOP is not significant and the secondary hydroxyls are reacting fast enough to incorporate SBOP into the PU network.

Foam made with SAN copolymer polyol has the highest extractable content and similar observations have been reported elsewhere [28]. The total concentration of SAN copolymer in 30% SAN is approximately 8 wt%. The 4.75% extractables observed can represent up to 60% of all SAN in the foam. The extractable fraction is likely comprised of SAN particles and the soluble components in SAN copolymer polyol. This is because SAN copolymer is synthesized via dispersion polymerization of styrene and acrylonitrile monomers in the presence of unsaturated polyether polyol as a stabilizing precursor [29–31]. Polymerized poly(styrene-*co*-acrylonitrile) forms discrete particles in foam while un-grafted and un-reacted monomers remain in the polyol mixture. Although the polymerized SAN particles are stabilized, no literature has reported on the chemical bond formation between the particle and the polyurethane network. The un-grafted copolymer and un-reacted monomers are incapable of chemical bonding and thus can be easily extracted [32].

3.2. Foam cellular structures

Performance of flexible foam requires high open cell content. Airflow (ASTM Standard D3574 Test G) is the standard

Table 2
IR band assignments in C=O region and peak area under the bands

	Ester carbonyl[a]	Free urethane	Free urea	Monodentate urea	Bidentate urea
Wavenumber (cm^{-1})	1745	1732	1713	1676, 1662	1645
Control	0.031	0.55	0.32	0.48	0.20
30% SAN	0.024	0.54	0.31	0.47	0.22
10% Crosslinker	0.020	0.57	0.42	0.42	0.16
10% SBOP	0.025	0.54	0.31	0.46	0.23
30% SBOP	0.080	0.60	0.31	0.44	0.25

All areas are normalized.
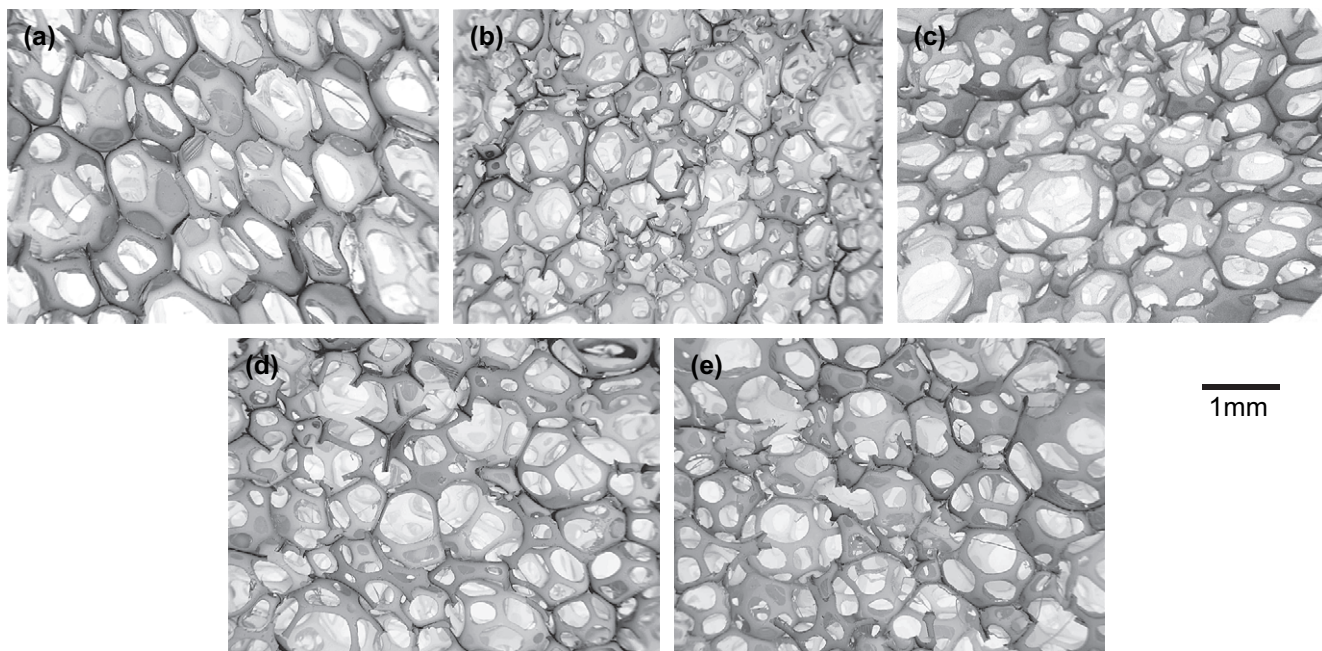[a] Calculated band area under ester carbonyl absorbance.

Fig. 3. SEM images: (a) control; (b) 30% SAN; (c) 10% crosslinker; (d) 10% SBOP and (e) 30% SBOP.

method measures cell openness. Sample foams were tested and the airflow data are shown in Table 1. All airflow values are within the standard range of open cell flexible foam [2]. Replacing base polyol with substituent polyols has little effect on cell openness.

The important parameters that affect mechanical properties of foams are cell strut thickness and length [1,2,33,34]. Because direct measurements of either parameter, strut thickness or length, can be subjective, we adopted the approach of measuring cell size [35–37]. Cell strut thickness and length can be estimated from measured cell size by using equations found in Ref. [33]. Generally, in open cell PU foams increased cell size increases foam modulus.

SEM micrographs like those shown in Fig. 3 were examined, and the average cell diameter and standard deviation obtained are shown in Fig. 4. The control foam has the largest average cell size and narrowest cell size distribution. With replacement of polyether polyol with crosslinker or SBOP, foam average cell size decreased and cell size distribution widened. Although it is seen in both SEM images and cell size analysis
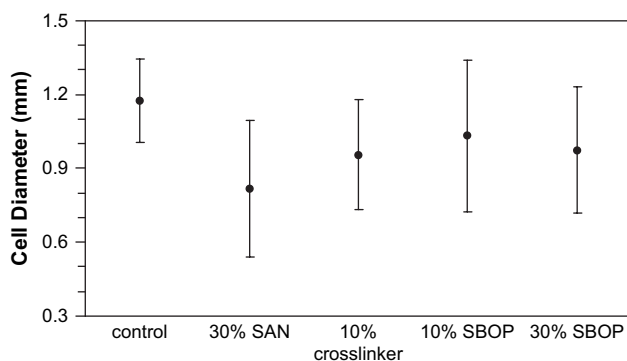

Fig. 4. Average cell diameter and standard deviation.

that SBOP and crosslinker foams have smaller cells, the size difference between either foam and control is not statistically significant. The change in SAN copolymer-containing foam is significant: the average cell size is 30% smaller than the control and cell size distribution is the broadest. However, the literature indicates that mechanical properties, such as compression modulus, will only change slightly by such change in size [35,38]. Thus the SEM study and cell size analysis suggest that partial substitution of polyols used here does not significantly alter cellular structure of the foam, and thus the observed foam mechanical properties' changes are unlikely to be due to cell size changes.

3.3. Polymer phase characterization

The polymer phase in a PU flexible foam comprises segmented block copolymer commonly denoted as $(A-B)_n$. The two blocks are a polyol and a polyurea. The incompatibility between the two blocks leads to a phase-separated morphology consisting of polyol-rich soft domains and polyurea-rich hard domains [39–41]. Both domains have a distinct glass transition temperature (T_g) and mechanical stiffness.

3.3.1. Dynamic mechanical analysis (DMA)

A direct approach to study the thermal and mechanical properties of the polymer phase is via DMA. Fig. 5 shows the modulus profiles of control, 30% SAN and 10% crosslinker foams. All three G' curves are similar up to their T_gs. At low temperatures, foams behave as a solid showing high G' values of 10^6 Pa. As temperature goes through T_g, a dramatic increase in molecular motion causes G' to decrease by nearly two orders of magnitude and reaches a plateau. Interestingly, the tan(δ) curves of all three foams (see Fig. 6) exhibit peaks at
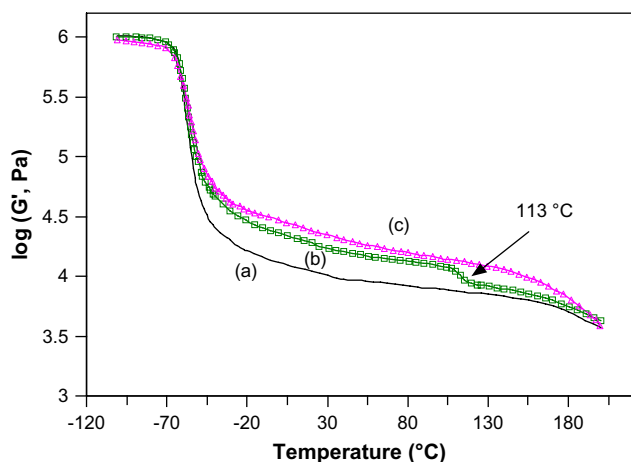
Fig. 5. DMA results: (a) control; (b) 30% SAN and (c) 10% crosslinker.

Fig. 7. DMA results: (a) control; (d) 10% SBOP and (e) 30% SBOP.

the same temperature. Thus, the soft phases in all three foams are polyether polyol-based soft phases with a T_g of $-56\,^\circ$C. At temperatures higher than the soft phase T_g, plateau moduli of the foams show appreciable differences. The plateau G' values of 30% SAN is 60% higher than the control, while the plateau G' values of foam with 10% crosslinker is 80% higher. Although increases of plateau modulus are seen in both SAN and crosslinker-substituted foams, the mechanisms for the increase are different. In both Figs. 5 and 6, 30% SAN foam clearly shows a second T_g at 113$\,^\circ$C and beyond this transition, improvement in the plateau G' vanishes. As alluded to earlier, SAN copolymer forms discrete particles and the T_g of polymerized SAN is approximately 120$\,^\circ$C [42]. SAN particles act as fillers in the polymer phase and thus improve foam plateau modulus. The observed increase in G', even after SAN particles soften, can be explained by a higher HS-to-SS ratio, shown in Table 2, in 30% SAN. In 10% crosslinker-substituted foam, improved plateau modulus extends over nearly the entire temperature range and is attributed to a higher concentration of HS [43]. This behavior will be further discussed in later sections.

Substitution with SBOP polyol, rather than simply elevating plateau modulus, alters the DMA profiles. A slow decay of
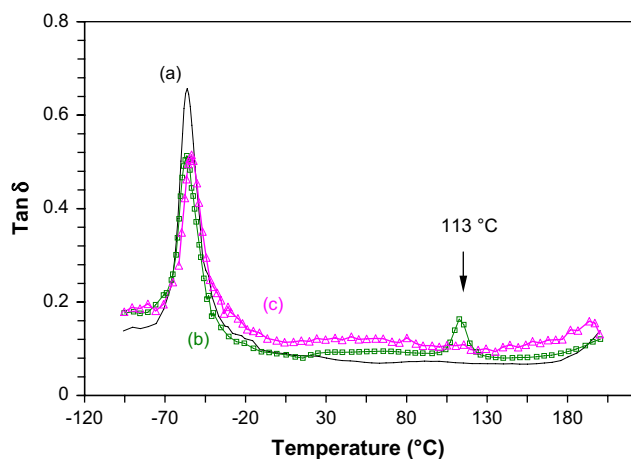
G' over a wide range of temperatures is seen in Fig. 7. Soft phase T_g of both SBOP foams determined from tan(δ) peaks remains the same as the control (Fig. 8), however, the tan(δ) peak heights are significantly reduced. In both SBOP foams, a large portion (70% and 90%) of the soft phase comprises polyether polyol-based SS; the smaller tan(δ) peaks indicate that these polyether polyol SS do not soften at their T_g. Especially in the case of 30% SBOP, the tan(δ) peak height is only one-third of the control implying a large population of polyether polyol SS is mixed with a higher T_g component, such as SBOP polyol. In Fig. 8, 30% SBOP foam shows a very broad tan(δ) peak around 75$\,^\circ$C; this could indicate a second, SBOP-containing soft phase. In addition to the loss of polyether polyol-based SS, the absence of plateau regions in both SBOP foams indicates the lack of defined distance between domain spacing. Both the continuous decrease in G' and the tan(δ) increase above 0$\,^\circ$C observed in SBOP foams argue for a distribution of phase sizes.

3.3.2. Differential scanning calorimetry (DSC)

DSC heating curves in Fig. 9 reaffirmed that all four substituted foams share the same soft phase T_g as that of the control. The DSC measured T_g is $-60\,^\circ$C (Fig. 10), very

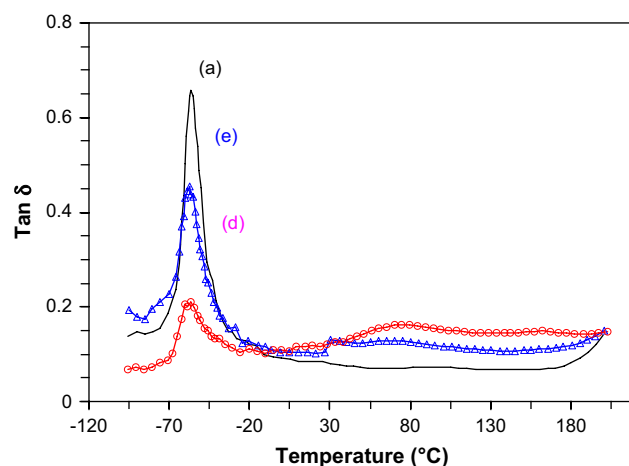Fig. 6. tan(δ) vs. temperature: (a) control; (b) 30% SAN and (c) 10% crosslinker.

Fig. 8. tan(δ) vs. temperature: (a) control; (d) 10% SBOP and (e) 30% SBOP.
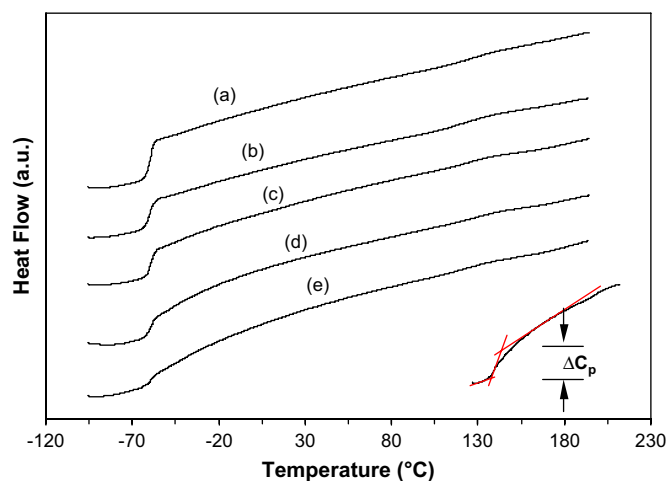
Fig. 9. DSC results: (a) control; (b) 30% SAN; (c) 10% crosslinker; (d) 10% SBOP and (e) 30% SBOP. The curves were shifted vertically to avoid overlapping of curves. Inset illustrates the method used to determine Δc_p and breadth of T_g.

similar to the temperature of the tan(δ) peaks. As discussed above the DMA results indicate that polyether polyol-based SS may have mixed with other components. DSC can quantify this. Since Δc_p scales with the total weight of polyether polyol-based SS undergoing a transition from a solid to a softened state, the weight fraction of pure polyether polyol soft phase can be estimated. The method for determining Δc_p is shown in the inset of Fig. 9 and the results are tabulated in Table 1.

Both SAN and crosslinker-substituted foams show a slight loss of the polyether polyol-based soft phase. The Δc_p values scale to 76% and 70% of control for crosslinker and SAN foams, respectively. Given the formulations in Table 1, 30% SAN should contain approximately 87% polyether polyol SS in its soft phase, while 10% crosslinker foam should contain 90% polyether SS in its soft phase. Clearly, substitution of crosslinker has more impact on the purity of the polyether polyol-based soft phase than SAN, but the impact is far less significant when compared to SBOP-substituted foams. The 10% and 30% SBOP foams contain 90% and 70% polyether SS in their soft phases, respectively, however, the measured Δc_p are only 48% and 42% of the control. Polyether SS in
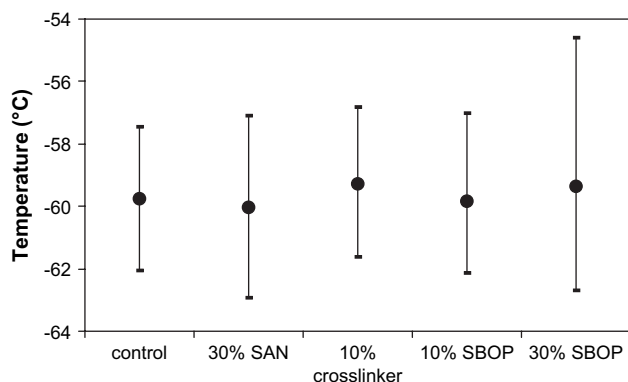
SBOP foams is not all phase-separated; a significant fraction of them is in a phase-mixed state with SBOP and/or HS.

To better understand the loss of polyether SS fraction, we also measured T_g of each pure polyol. The T_gs of control, SAN-containing, crosslinker, and SBOP polyols are −68, −68, −51, and −35 °C, respectively. SBOP obviously has a much higher T_g than the other polyols.

3.3.3. Small-angle X-ray scattering (SAXS)

SAXS was used to determine interdomain spacing, as well as, to probe the degree of phase separation. SAXS profiles of foam samples are shown in Fig. 11. The interdomain spacing of 10% crosslinker (127 Å) is notably greater than that of control (115 Å), while other samples remain similar to the control. Scattering signal intensity is notably different between foams. SAN (30%) clearly has an enhanced signal intensity, while the two SBOP-containing foams show great reductions in signal intensities.

Normalized SAXS intensity is affected by two main parameters: (1) the number of scattering objects, which is related to the volume fraction and also weight fraction of hard domains (electron dense phase) and (2) the inherit electron density contrast between the hard and soft domains [44,45]. The observed increase in intensity of 30% SAN is attributable to the former, a higher volume fraction of hard domains/scattering objects. This is because the HS-to-SS ratio is higher in the 30% SAN polymer phase than the control. On a per volume basis, there are more scattering surfaces in SAN-containing foam than in the control. Crosslinker and SBOP foams all have higher HS concentrations compared to control, however, SAXS intensities are much lower.

Crosslinker foam, in addition to signal intensity loss, showed a visible interdomain spacing increase of over 10 Å. Since the bulk of the soft domains is still polyether polyol-based, the interdomain spacing change is likely achieved via an increase in hard domain size. Low molecular weight crosslinker polyols can mix with the HS and form swelled hard
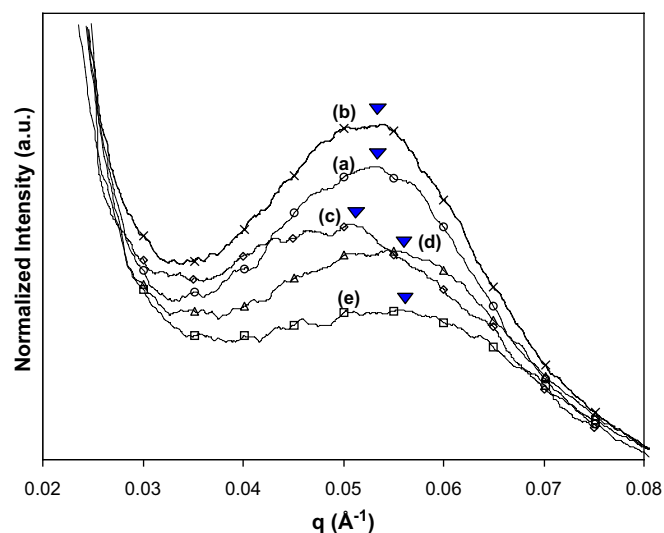

Fig. 10. DSC results: the dots indicate the glass transition temperatures. Upper and lower bars indicate the breadth of the transition.

Fig. 11. Scattering profiles of foams obtained using SAXS: (a) control ($\bigcirc$); (b) 30% SAN ($\times$); (c) 10% crosslinker ($\diamond$); (d) 10% SBOP ($\triangle$) and (e) 30% SBOP ($\square$). Inverted triangles indicate average interdomain spacings.

domains, consequently, a larger hard domain size gives rise to a larger interdomain spacing [46–49]. In addition, hard domains swelled with crosslinker polyol are lower in electron density than un-swelled hard domains. Therefore, the electron density contrast between soft and hard domains is reduced and 10% crosslinker foam shows a reduction in SAXS intensity.

Substitution of SBOP has the most significant impact on SAXS intensity. Both scattering profiles of SBOP-containing foams show a slight decrease in interdomain spacing (higher q value) and great reductions in signal intensity. The reduction in intensity also increases as concentration of SBOP and HS increases. Implicitly, substitution of SBOP reduces the electron density difference between the hard and soft domains. Three possible scenarios are considered. First, the SBOP could mix into the hard domains, thus "diluting" electron density contrast. However, unlike in the case of 10% crosslinker foam, SBOP samples showed no signs of increase in interdomain spacing (low q values). In fact, a small shift of the scattering profile to higher q values is observed. Thus, SBOP does not seem to swell hard domains like the crosslinker does. A second possibility is that HS is phase mixed with SS, where the hard domain is replaced by non-hydrogen-bonded HS. In such a case, it would reduce the SAXS intensity. However, the results of a FTIR study, presented in a later section, indicate HS in SBOP foams is well associated through hydrogen bonding. A third possibility is that rather than forming well-defined large hard domains, smaller hard domains may have replaced these large ones in the SBOP foams. A wide distribution of interdomain spacing could lead to a reduction in SAXS intensity. Additionally, smaller hard domain size equates to more interfacial areas per unit volume, which may explain the loss of SS observed in SBOP foams.

3.3.4. Atomic force microscopic (AFM) images

So far, all experiments are indirect measures to the polymer phase morphology. It is desirable to "see" the hard and soft domains and thus understand the changes in morphology due to substituent polyols. This is possible using AFM.

Phase images of foams acquired via AFM are shown in Fig. 12. Hard and soft domains are indicated by different colors. Yellow-to-white (light) colored areas correspond to high modulus regions, i.e., hard domains, and brown-to-black (dark) colored areas correspond to low modulus regions, i.e., soft domains. The hardness difference between two domains is correlated to a phase scale expressed in degrees [50,51]. For each image, the overall phase scale was adjusted to clearly illustrate foam morphology, as indicated in the caption of Fig. 12. During tapping mode image acquisitions, the AFM tip was controlled to indent the sample surface by approximately 15 nm. By controlling the distance of tip–sample interaction, comparison of phase images can be made more consistently.

Control foam in Fig. 12a clearly shows a two-phase, well-separated morphology. Each phase is distinguishable by color and the boundaries are visible. The image is displayed at a total phase scale of 25°, which is similar to previous findings by other studies [50,52]. A higher magnification image of the control sample in Fig. 12b showed an estimated interdomain

spacing of 100–150 Å, which is in good agreement with inter-domain spacing measured in SAXS, 115 Å.

Phase images (not shown here) of SAN-containing sample exhibited the same phase-separated morphology and domain spacing as the control. In addition, 30% SAN foam also exhibits a unique feature — SAN particles dispersed within the polymer phase as shown in Fig. 12c and d. These are SAN particles because they are: (1) spherical in shape (different from the hard domains seen in the control), (2) large in size and (3) high in modulus. The measured diameters of these particles range from 0.2 to 0.7 μm, consistent with the known composition and specification of Hyperlite® E-849 copolymer polyol. The hardness difference between these particles and soft domains is much higher than that between hard and soft domains. The overall image phase scale is 90° for Fig. 12c and d. It is interesting to note that samples compressed at 120 °C lost this large-scale morphology presumably due to flow of the SAN particles.

Phase images of 30% SBOP display quite different morphology from the control. Phase images in Fig. 12e and f were taken at two different regions of the same sample, showing morphology variation within 30% SBOP. The most noticeable feature is that the domain boundaries in Fig. 12e–h are blurry. In addition, a size variation of hard domains can be seen in these images. In Fig. 12e and f, some hard domains have slightly more distinguishable boundaries while the rest do not. From a sampling of different regions on 30% SBOP foam and previous results in DMA, the slightly better phase-separated areas could be polyether polyol-based soft domain rich region. Phase images in Fig. 12e and f are displayed with an overall phase scale of 25° and the measured average phase hardness difference is only 10°. This signifies that the modulus of the soft domains increased. A similar, but more pronounced drop in phase hardness difference is observed in Fig. 12g and h. The overall phase scale is 10° and measured phase hardness difference is less than 8°. The boundaries here between the two phases are even less detectable. More importantly, hard domains appear to be smaller in size than those seen previously, especially in control.

The AFM images of 30% SBOP foam show that hard domains are smaller in size, in close proximity, and have no clear boundaries. The hardness difference between the soft and hard domains is significantly less in SBOP foams. It is expected that the 30% SBOP foam has a higher overall room temperature modulus than other foams because the soft domains in SBOP foam are relatively harder. Two possible reasons may contribute to the higher modulus in SBOP foam. First, the reduced hard domain size and loss of domain boundaries. This may influence the soft phase by increasing HS/SS interface thus trapping SS at interfaces and reducing the amount of SS participating in soft domains. Second, the SBOP-based soft domain is harder. In Section 3.3.1, we speculated that there may exist a second soft phase rich with SBOP-based SS and a T_g around 75 °C.

The blurred boundaries between hard and soft domains in 30% SBOP foam also raise a question whether the amount of hydrogen bonding between HS has been altered. The following section of FTIR-ATR examines the amount of
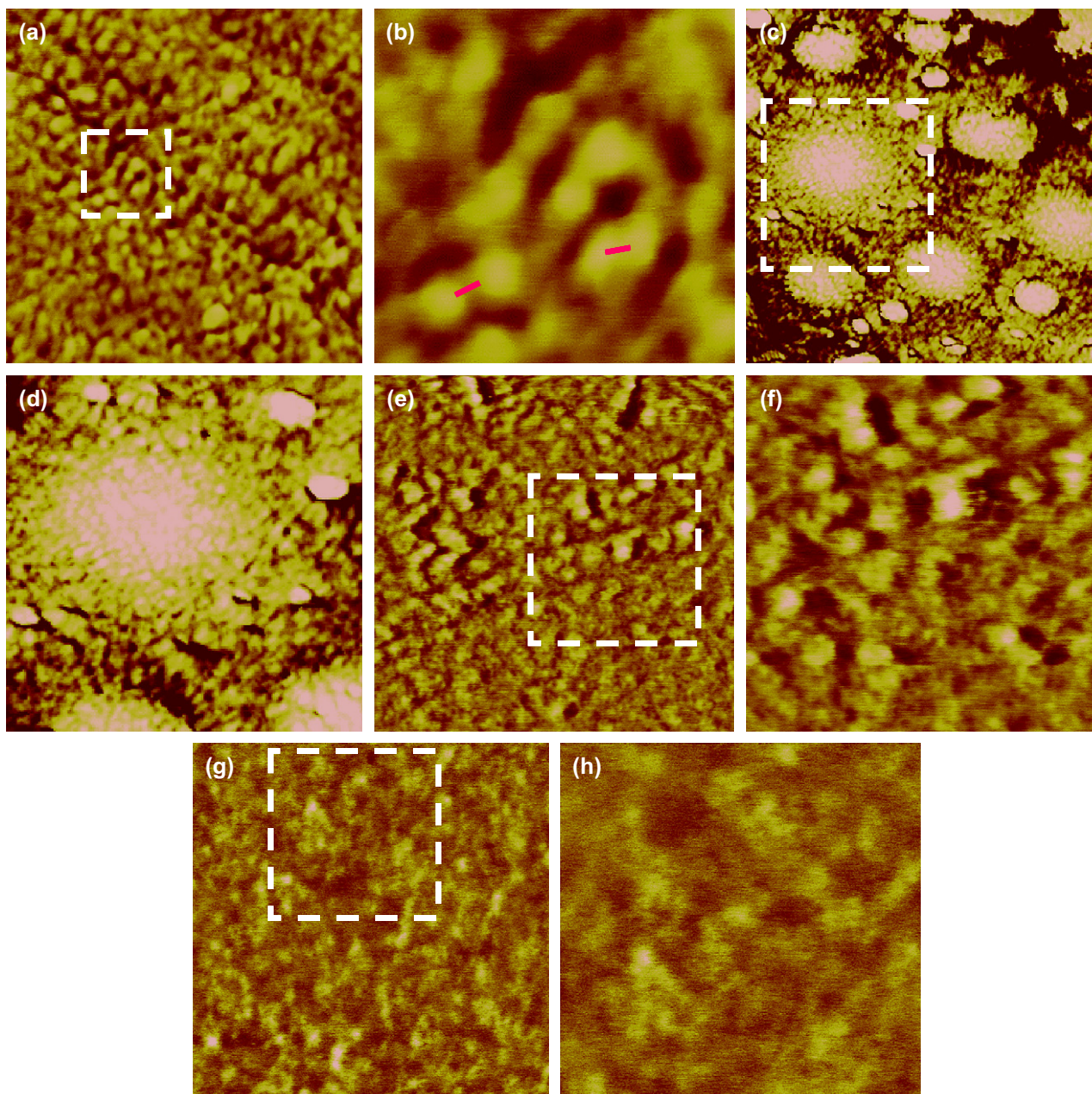
Fig. 12. Tapping mode AFM images. Images (b), (d), (f) and (h) are higher magnifications of the indicated regions on images (a), (c), (e) and (g) respectively. Colored bars in (b) are 100 Å in length: control (a) 1×1 mm, 25°-scale, (b) 250×250 nm, 25°-scale, 30% SAN (c) 2×2 mm, 90°-scale, (d) 1×1 mm, 90°-scale, 30% SBOP (e) 1×1 mm, 25°-scale, (f) 500×500 nm, 25°-scale, 30% SBOP (g) 1×1 mm, 10°-scale, (h) 500×500 nm, 10°-scale.

hydrogen-bonded species and molecular differences between substituted foams.

3.3.5. Fourier transform infrared (FTIR) spectroscopy with attenuated total reflectance (ATR)

FTIR-ATR spectra of the foams' carbonyl regions (1550−1800 cm^{-1}) are shown in Fig. 13. Two particular absorbance regions are of interest: free species region, >1700 cm^{-1}, comprising both free urethane and free urea, and H-bonded species region, <1700 cm^{-1}. Details of spectra interpretation and band assignments can be found in Refs. [53−55]. These bands are listed in Table 2 along with the peak areas.

Polyurea HS that does not participate in hard domain formation remains in the polymer as free, i.e., non-hydrogen-bonded urea. These free ureas have an IR absorbance at 1713 cm^{-1}. Among all foam samples shown in Fig. 13, 10% crosslinker shows the highest free urea absorbance band while very little variation in free urea absorbance band is seen in the other foams. These free ureas are likely the result of swelled hard domains, which agrees with the increase in interdomain spacing observed by SAXS (Fig. 11).

The state of urethane bond provides less information on phase morphology, nevertheless, urethane still participates in hydrogen bonding via its carbonyl group. In general, more
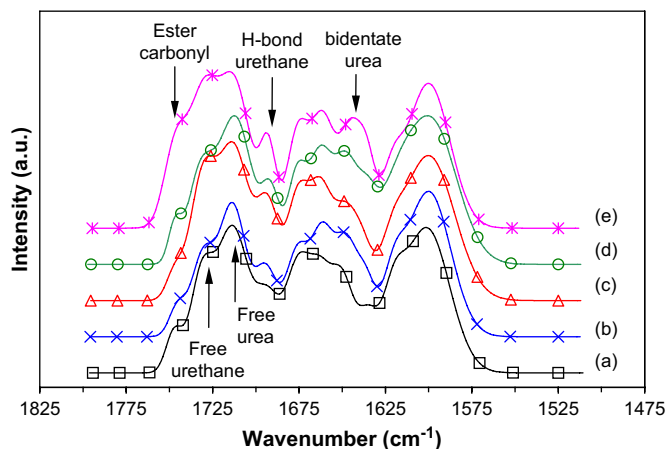
Fig. 13. ATR-IR spectra of the carbonyl region: (a) control (□); (b) 30% SAN (×), (c) 10% crosslinker (△); (d) 10% SBOP (○); and (e) 30% SBOP (✳). Spectra are offset vertically.
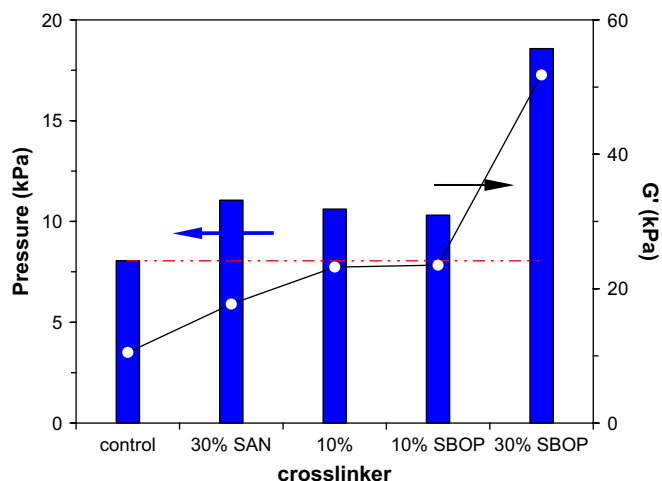

Fig. 14. Column data show compression properties of foams, reported as pressure required to achieve 65% compression (ASTM D 3574-95, test B1). All samples showed increases of compression pressure over control (dotted line). Line data show shear modulus, G', measured at 25 °C.

than half of the urethane bonds remain free [56]. Our foam samples show some variation in free urethane content. SAN (30%) and SBOP (10%) have the least amount of free urethane followed by control, 10% crosslinker and 30% SBOP. Other than the 10% SBOP sample, the free urethane amount increases with increasing molar concentration of hydroxyls in the formulation. Note that 30% SAN and 10% SBOP closely resembles each other in the urethane composition.

Hydrogen-bonded ureas, including both monodentate and bidentate, are indications of hard domain ordering. The structure of monodentate urea is less ordered than that of bidentate urea. From control, 30% SAN, 10% SBOP to 30% SBOP, the absorbance bands shift from monodentate to bidentate urea. The shift in hydrogen-bonded urea region is in agreement with HS concentrations tabulated in Table 1 and is possibly a result of concentration effect. However, 10% crosslinker has the second highest HS concentration, and its IR spectrum shows the lowest bidentate urea absorbance. HS in 10% crosslinker is evidently not well associated and ordering in hard domains has been disrupted. The two SBOP-substituted foams are quite unique. The spectrum of 10% SBOP foam, as with the urethane spectrum region, resembles 30% SAN in the urea species composition. The similarity between the two spectra, 30% SAN and 10% SBOP, indicates that substituting copolymer filler or SBOP may have a similar effect on morphology. In 30% SBOP foam, the hard domains are more ordered. The peak at 1645 cm^{-1} is more evident in the spectrum of 30% SBOP than in the others. Although the AFM and SAXS indicate that hard domains are smaller, FTIR indicates that the HS ordering within these domains is improved over the control. The bidentate urea peak in SBOP foam elucidates that SBOP plays a different role in polymer phase morphology from crosslinker.

3.3.6. Indentation force deflection (IFD)

The compressive properties of foams were evaluated using IFD tests and results are both plotted in Fig. 14 and tabulated in Table 1. All substituent polyols have improved compression pressure considerably over the control. Conventional

approaches to improve foam compression properties using copolymer-filled polyol and crosslinker showed approximately 35% increase in compression pressure. A similar amount of increase was achieved with 10% substitution using SBOP. When the amount of substituent SBOP increased to 30%, a startling 131% increase is observed. The more-than-doubled increase in compression pressure is a result of higher modulus of the foam polymer phase. A side-by-side comparison of foam shear modulus G' at 25 °C and compression pressures measured in IFD tests are shown in Fig. 14.

4. Conclusions

The experimental results demonstrated that the substituent polyols used in this study are all capable of improving mechanical properties, specifically compressive properties. However mechanisms, through which the increases were achieved, are different.

Substituting SAN copolymer-filled polyol results in slightly smaller cell size and does not change phase-separated morphology in the polymer phase. The increase in IFD test is correlated to a higher polymer phase modulus as a result of SAN particles acting as reinforcement.

The use of the crosslinker polyol alters polymer phase morphology, especially that of hard domains. This low molecular weight polyol mixes into the hard domains, disrupts hard domain ordering and alters interdomain spacing. Significant loss of HS to free ureas has been shown to result in reduction in modulus [56,57]. However, the overall concentration of HS in 10% crosslinker foam compensates for its loss of hard domain ordering. The improved modulus, thus higher IFD, is a result of higher HS concentration.

SBOP foams have the most interesting results. Although it is a low molecular weight polyol, the SBOP-substituted foam is morphologically different from its petroleum counterpart,

crosslinker foam. The thermal analysis, DSC and DMA, shows that SBOP foams have much less than the expected amount of polyether soft domains. The DMA results further suggest that there may exist an SBOP-rich region in SBOP foams, which has a higher T_g than the polyether polyol-based soft domains. AFM images verify the possibility of two types of soft domains. In addition, AFM images show that 30% SBOP has smaller hard domains with a distribution of interdomain spacings. The observed broad peak in SAXS is, therefore, due to lower electron density contrast between hard and soft domains and a broad interdomain spacing distribution. The FTIR results indicate that SBOP-containing foams have the most ordered hard domain structures, implying a well phase-separated hard phase.

The improved polymer modulus in SBOP foam is attributed to a combination of factors: a high T_g SBOP-rich phase, high HS concentration, and improved hard domain ordering.

Acknowledgements

References

[1] Szycher M. Szycher's handbook of polyurethanes. Boca Raton: CRC; 1999.
[2] Herrington R, Hock K, editors. Flexible polyurethane foams. 2nd ed. Midland: Dow Chemical Co.; 1997.
[3] U.S. Department of Energy, Petroleum Marketing Monthly; Feb 2007.
[4] U.S. Department of Agriculture, Monthly feedstuff prices and peanut report; Feb 2007.
[5] Schaefer BF. Science 2005;308:1267.
[6] Lysenko Z, Morrison DL, Babb DA, Bunning DL, Derstine CW, Gilchrist JH, et al. WO Patent 2004096744 A2; 2004.
[7] Petrovic Z, Javni I, Guo A, Zhang W. US Patent 6,433,121; 2002.
[8] Petrovic ZS, Zhang W, Javni I. Biomacromolecules 2005;6:713–9.
[9] Hou CT. Adv Appl Microbiol 1995;41:1–23.
[10] Suresh KI, Kishanprasad VS. Ind Eng Chem Res 2005;44:4504–12.
[11] Javni I, Petrovic ZS, Guo A, Fuller R. J Appl Polym Sci 2000;77:1723–34.
[12] Javni I, Zhang W, Petrovic ZS. J Appl Polym Sci 2003;90:3333–7.
[13] Randall D, Lee S, editors. The polyurethanes book. John Wiley & Sons, Ltd.; 2002.
[14] Chian KS, Gan LH. J Appl Polym Sci 1998;68:509–15.
[15] Hu YH, Gao Y, Wang D-N, Hu CP, Zu S, Vanoverloop L. J Appl Polym Sci 2002;84:591–7.
[16] Guo A, Javni I, Petrovic ZS. J Appl Polym Sci 2000;77:467–73.
[17] Nozawa K, Sasaki M, Okubo K. Proceedings of polyurethane technical conference and trade fair. Houston, TX; 2005. p. 50–6.
[18] John J, Bhattacharya M, Turner RB. J Appl Polym Sci 2002;86:3097–107.
[19] Herrington R, Malsam J. US Patent Application 2005/0070620; 2006.
[20] Lysenko Z, Babb DA, Stutts KJ, Robbyn P, Zhang M, Schrock AK. WO Patent 2006118995 A1; 2006.
[21] Babb D, Phillips J, Keillor C. Proceedings of polyurethanes technical conference. Salt Lake City, UT; 2006. p. 189–93.
[22] Bayer Material Science NAFTA, http://www.bayermaterialsciencenafta.com/products/ [accessed on: July 10th, 2007].
[23] Dow Chemical Company, http://www.dow.com/polyurethane/na/product/ [accessed on: July 10th, 2007].
[24] Han X, Zeng C, Lee JL, Koelling KW, Tomasko DL. Polym Eng Sci 2003;43:1261–75.
[25] Rhodes MB, Khaykin B. Langmuir 1986;2:643–9.
[26] Corbett GE, Wadie BJ. J Elastom Plast 1973;5:180–95.
[27] Pechar TW, Sohn S, Wilkes GL, Ghosh S, Frazier CE, Fornof A, et al. J Appl Polym Sci 2006;101:1432–43.
[28] Kaushiva BD, Dounis DV, Wilkes GL. J Appl Polym Sci 2000;78:766.
[29] Ramlow GG, Pizzini LC, Patton Jr JT, Murphy JR. US Patent 4,014,846; 1977.
[30] Van Cleve R, Armstrong GH, Simroth DW. US Patent 4,242,249; 1980.
[31] Shriniwas CS. US Patent Application 0025492; 2006.
[32] Guo R, Lu X, Hua M, Fang D, Yao K. Polym Int 2001;50:1379–83.
[33] Gibson LJ, Ashby MF. Cellular solids: structure and properties. Elmsford, New York: Pergamon Press Inc.; 1988.
[34] Shutov FA. In: Klempner D, Frisch KC, editors. Polymeric foams. Munich: Hanser; 1991.
[35] Blair EA. Resinography of cellular plastics. In: A symposium presented at the sixty-ninth annual meeting. American society for testing and materials, Atlantic City, NJ. June 26–July 1, 1966. ASTM special technical publication, vol. 414. Philadelphia: American Society for Testing and Materials; 1967.
[36] Shutov FA. Adv Polym Sci 1983;51:155–218.
[37] Rhodes MB. In: Hilyard NC, Cunningham A, editors. Low density cellular plastics. New York: Chapman & Hall; 1994.
[38] Rusch KS. J Appl Polym Sci 1969;13:2297–311.
[39] Noshay A, McGrath JE. Block copolymers: overview and critical survey. New York, San Francisco, London: Academic Press; 1977.
[40] Macosko CW. RIM: fundamentals of reaction injection molding. Munich, New York: Hanser Publishers; 1989.
[41] Cooper SL, Tobolsky AV. J Appl Polym Sci 1966;10:1837–44.
[42] Dlubek G, Pionteck J, Kilburn D. Macromol Chem Phys 2004;205:500–11.
[43] Gier DR, O'Neill RE, Adams MR, Priester RDJ, Lidy WA, Barnes CG, et al. Proceedings of polyurethanes expo. Dallas, TX; 1998. p. 227–37.
[44] Stout GH, Jensen LH. X-ray structure determination. New York: The Macmillan Company; 1968.
[45] Velankar S, Cooper SL. Macromolecules 1998;31:9181–92.
[46] O'Sickey MJ, Lawrey BD, Wilkes GL. Polymer 2002;43:7399–408.
[47] Kaushiva BD, Wilkes GL. J Appl Polym Sci 2000;77:202–16.
[48] Kaushiva BD, Wilkes GL. Polymer 2000;41:6981–6.
[49] Li W, Ryan AJ, Meier IK. Macromolecules 2002;35:6306–12.
[50] McLean RS, Sauer BB. Macromolecules 1997;30:8314–7.
[51] Garrett JT, Runt J, Lin JS. Macromolecules 2000;33:6353–9.
[52] Kaushiva BD, Wilkes GL. Polymer 2000;41:6987–91.
[53] Yilgor E, Yilgor I, Yurtsever E. Polymer 2002;43:6551–9.
[54] Luo N, Wang DN, Ying SK. Macromolecules 1997;30:4405.
[55] Elwell MJ, Ryan AJ, Grunbauer HJM, Van Lieshout HC. Macromolecules 1996;29:2960–8.
[56] Seymour RW, Estes GM, Cooper SL. Macromolecules 1970;3:579–83.
[57] Garrett JT, Xu R, Cho J, Runt J. Polymer 2003;44:2711–9.